https://doi.org/10.5194/essd-2024-187
Preprint. Discussion started: 3 June 2024

Open Access Earth System Science Data Discussions

An integrated dataset of ground hydrothermal regimes and soil nutrients monitored during 2016-2022 in some previously burned areas in hemiboreal forests in Northeast China

Xiaoying Li [1], Huijun Jin [1, 2, 3] *, Qi Feng [4], Qingbai Wu [1], Hongwei Wang [1, 2], Ruixia He [1], Dongliang Luo [1], Xiaoli Chang [1, 5], Raul-David Șerban [6], and Tao Zhan [3]

[1] Key Laboratory of Cryospheric Science and Frozen Soil Engineering, Northwest Institute of Eco-Environment and Resources, Chinese Academy of Sciences, Lanzhou 730000, China;

[2] School of Civil Engineering and Transportation, China-Russia Joint Laboratory of Cold Regions Engineering and Environment, and Permafrost Institute, Northeast Forestry University, Harbin 150040, China;

[3] Ministry of Natural Resources Field Observation and Research Station of Permafrost and Cold Regions Environment in the Da Xing'anling Mountains at Mo'he, Natural Resources Survey Institute of Heilongjiang Province, Harbin 150036, China;

[4] Key Laboratory of Ecohydrology of Inland River Basin, Northwest Institute of Eco-Environment and Resources, Chinese Academy of Sciences, Lanzhou 730000, China;

[5] Hunan University of Science and Technology, Xiangtan, Hunan 411202, China and;

[6] Faculty of Agricultural, Environmental and Food Sciences, Free University of Bozen-Bolzano, Bolzano 39100, Italy

* Corresponding authors: Huijun Jin (hjjin@nefu.edu.cn) at the School of Civil Engineering and Transportation, Northeast Forestry University, Harbin 150040, China

Abstract:

Under a warming climate, occurrences of wildfires have been increasingly more frequent in boreal and arctic forests during the last few decades. Wildfires can cause radical changes in the forest ecosystems and permafrost environment, such as irreversible degradation of permafrost, successions of boreal forests, rapid and massive losses of soil carbon stock, and increased periglacial geohazards. Since 2016, we have

https://doi.org/10.5194/essd-2024-187
Preprint. Discussion started: 3 June 2024

gradually and more systematically established a network for studying soil nutrients and monitoring the hydrothermal state of the active layer and near-surface permafrost in the northern Da Xing'anling (Hinggan) Mountains in Northeast China. The dataset of soil moisture content (0-9.4 m in depth), soil organic carbon (0-3.6 m), total nitrogen (0-3.6 m), and total phosphorus and potassium (0-3.6 m) have been obtained by field sampling and ensuing laboratory tests. Long-term datasets (2017-2022) of ground temperatures (0-20 m) and active layer thickness have been observed by thermistor cables permanently installed in boreholes. The present data can be used to simulate changes in permafrost features under a changing climate and wildfire disturbances and to explore the changing interactive mechanisms of the fire-permafrost-carbon system in the hemiboreal forest. Furthermore, they can provide baseline data for studies and action plans to support the carbon neutralization initiative and assessment of ecological safety and management of the permafrost environment. These datasets can be easily accessed from the National Tibetan Plateau/Third Pole Environment Data Center (https://doi.org/10.11888/Cryos.tpdc.300933, Li and Jin, 2024).

1 Introduction

As a key component of the Northern Hemisphere, permafrost and its changes can have substantial consequences for natural and man-made systems (Smith et al., 2022). Moreover, due to its high sensitivity to climate warming, surface disturbances, and human activities, permafrost has undergone extensive degradation during the last six decades (e.g., Biskaborn et al., 2019; Chang et al., 2022; Jin et al., 2000, 2007, 2021, 2022, 2023; Li et al., 2022a; Petrov et al., 2022). As one of the most common natural agents and disturbance factors in boreal forests and arctic tundra, wildfires can initiate ecosystem renewal at different spatiotemporal scales (Chen et al., 2021; Johnstone et al., 2004; Li et al., 2019). Wildfires impact the permafrost environment first by modifying or altering the ground hydrothermal regimes (Jorgenson et al., 2013; Li et al., 2022b; Yoshikawa et al., 2003), and subsequently by inducing modifications or radical/irreversible changes in biogeochemical processes (e.g., Fultz et al., 2016; Li et

https://doi.org/10.5194/essd-2024-187
Preprint. Discussion started: 3 June 2024

al., 2023; Ping et al., 2010; Xu et al., 2024). In boreal forests and arctic tundra, wildfires have become increasingly more frequent in recent decades under a warming climate and increasing human activities (Boyd et al., 2023; Chen et al., 2023; French et al., 2015; Knorr et al., 2016; Westerling et al., 2006).

In boreal regions, vegetation and organic layer are essential buffering and protective layers of the underlying active layer and permafrost. The combustion of all vegetation cover and partial or complete removal of the insulating organic layer have a direct impact on permafrost. It reduces the land surface albedo, increases ground surface and cryosol/ice exposure to direct solar radiation, and weakens the shading effect of vegetation and evapotranspirative cooling effect (Johnstone et al., 2010; Nossov et al., 2013; Shur and Jorgenson, 2007; Yoshikawa et al., 2003). All of these contribute to higher ground surface temperature and more heat transferred into the ground, resulting in a rapid ground warming and sharp deepening of the active layer (Li et al., 2022b; Michaelides et al., 2019; Nossov et al., 2013; Smith et al., 2015). Post-fire ground warming and subsequent thawing of permafrost lead to the formation of massive thermokarst phenomena and extensive occurrences of periglacial geohazards or landforms (Brown et al., 2015; Fedorov and Basharin, 2022; Kokelj and Jorgenson, 2013; Yoshikawa et al., 2003), such as ground surface subsidence and thaw settlement, retrogressive thaw slumps (Balser et al., 2014; Kokelj et al., 2009), slope instability (Gruber and Haeberli, 2007), active-layer detachment failures (Lewkowicz et al., 2011; Lewkowicz and Harris, 2005), and changes in hydrological processes (Ackley et al., 2021; Kopp et al., 2017; Miner et al., 2022).

In addition to the abrupt and rapid degradation of permafrost and extensive formation of thermokarst, wildfire disturbance also has important and long-term ramifications for terrestrial carbon cycling and carbon stocks (Chen et al., 2022). Unlike gradual thawing, abrupt changes in ground hydrothermal regimes often disrupt the entire soil profile and initiate or aggravate carbon loss from deep permafrost soils (Jones et al., 2015; Turetsky et al., 2019). Therefore, the combustion of vegetation and the subsequent thawing of ecosystem-protected permafrost have resulted in a rapid release

https://doi.org/10.5194/essd-2024-187
Preprint. Discussion started: 3 June 2024

of large amounts of carbon into the atmosphere as greenhouse gases (Mack et al., 2011, 2021). Furthermore, over a short time, abrupt permafrost thaw and the ensuing thermokarst would possibly result in emitting more methane than gradual thaw (Koven et al., 2015). As a result, the fire-induced increase in carbon emissions may have strong positive feedbacks on climate warming at different scales (Koven et al., 2015).

Located on the southern margin of Eastern Asian hemiboreal forests and permafrost zones, the Da Xing'anling (Hinggan) Mountains in Northeast China are prone to frequent and massive wildfires. The Xing'an permafrost here is controlled or strongly affected by many local factors, such as dense vegetation cover, thick organic layer, stable snow cover, and anthropic development (Jin et al., 2007; Şerban et al., 2021; Wang et al., 2024). The ecosystem-dominated (driven, modified, or protected) permafrost is very sensitive to climate warming and prone to wildfires (Shur and Jorgenson, 2007). However, prior to the early 1980s, there was little research on wildfire impacts on the permafrost environment in Northeast China. There were only a few occasional fire-related geocryological studies in the early 1990s and limited site-specific measurements of soil temperature and moisture content in the active layer and near-surface (≤20 m in depth) permafrost near the Amu'er town, northern Heilongjiang Province (Liang et al., 1991; Zhou et al., 1993). Moreover, research on fire impacts on soil carbon and nitrogen pools and cycles in the Xing'an permafrost in Northeast China has just started and still at its fledgling stage. Due to the cold and arid climate in winter and spring, complex mountain topography, and dense hemiboreal vegetation in the region, fire regimes are often complex. In addition, burned areas are often located in pristine forest areas far away from roads, making it challenging to timely and/or readily access and study. Therefore, it is difficult to systematically understand and quantitatively evaluate the effects of wildfires on ground hydrothermal regimes and carbon stocks at different spatiotemporal scales (Li et al., 2021).

To address the abovementioned issues, since 2016, a continuous observation system has been gradually established for ground hydrothermal regimes and soil nutrient contents in the northern Da Xing'anling Mountains. This dataset can provide

https://doi.org/10.5194/essd-2024-187
Preprint. Discussion started: 3 June 2024

important supportive data for studying permafrost landscapes, carbon stocks, and boreal ecology and hydrology. It can also provide important references for the management of land and water resources and ecological environment after wildfire disturbances in Northeast China, particularly in forested hemiboreal permafrost regions. In Section 1 of this paper, we first introduce the comprehensive observation network of permafrost and soil nutrients in the northern Da Xing'anling Mountains. The design of the monitoring network of ground hydrothermal regimes and systematic observations of soil nutrient contents, and evaluation of data quality are given in Section 2. In Section 3, observations of permafrost hydrothermal regimes and soil nutrients that provide a 6-year-long dataset are described and briefly interpreted with a focus on the major features of the observation network for better understanding of the dataset structure and contents. The data availability and accessibility are provided in Section 4, and; in Section 5, major conclusions and prospects are provided. This dataset provides important input for the model simulations of permafrost changes under fire disturbances and a warming climate, especially those rapid and abrupt degradation of the Xing'an permafrost and resultant periglacial phenomena, such as thermokarst, thaw settlement, and ground surface subsidence and ponding. It is useful for analyzing the interactive hydrothermal and cyclic mechanisms of the wildfires-permafrost-carbon system in the hemiboreal forest.

2 Monitoring networks and data processing

2.1 Study area descriptions and monitoring networks

A permafrost monitoring network has been established in four burned areas in the northern Da Xing'anling Mountains in Northeast China (Figure 1). Two are located in shrub wetlands in Mo'he city (MH) and Gulian town (GL) in northern Heilongjiang Province. The other two are located in larch forests in Alongshan (AL) and Mangui towns (MG) in the northeastern part of Inner Mongolia. The network includes eight sites in the four burned areas with two fire severity (severely burned (S) and unburned (U)) from 1987 to 2015. The studied forest fire in MH (with severely burned (MH-S) and unburned (MH-U) sites) occurred on 6 May 1987, with a burned-over area of

https://doi.org/10.5194/essd-2024-187
Preprint. Discussion started: 3 June 2024

1.01×10^6 hm^2; that in GL (with severely burned (GL-S)) and unburned (GL-U) sites), on 28 July 2002, 1,121 hm^2; AL (with severely burned (AL-S) and unburned (AL-U) sites), on 10 May 2009, 930 hm^2, and; MG (with severely burned (MG-S) and unburned (MG-U) sites), on 12 July 2015, 237 hm^2.

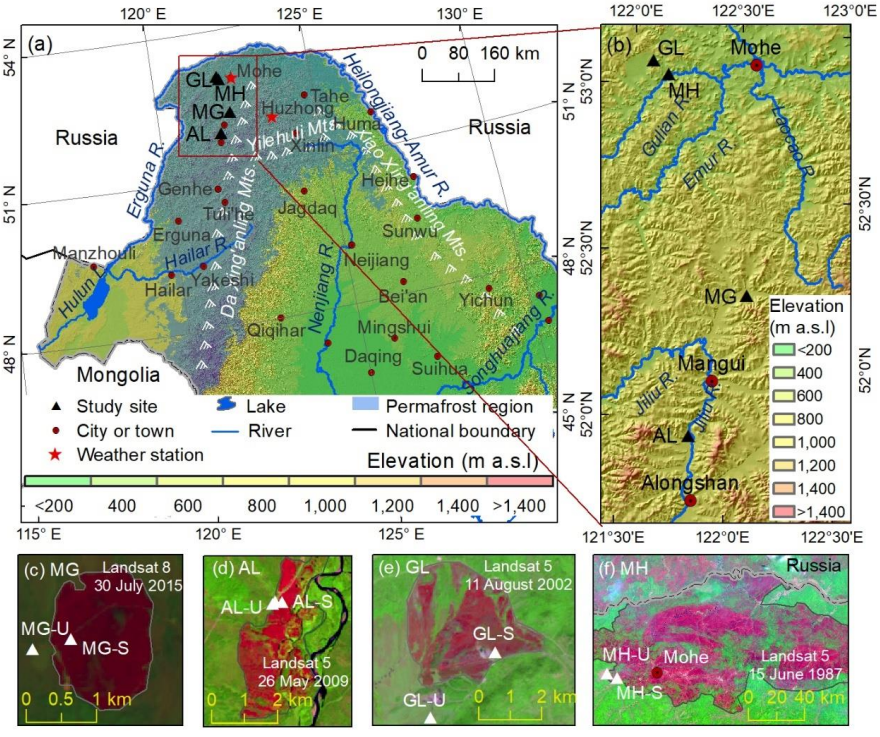

Figure 1. Location of the study areas and sites in the northern Da Xing'anling Mountains, Northeast China. The base map of permafrost distribution is modified from Li et al. (2022c)

The study areas are characterized by a cold temperate continental climate. In the study areas of GL and MH, based on the data of nearby Mo'he weather station from 1960 to 2020, mean annual air temperature (MAAT) ranged from −6.2 to −2.4°C, with an average rate of climate warming at 0.3°C per decade; annual precipitation was 274~675 mm, with a slight average wetting trend of 13.8 mm per decade. In the study areas of MG and AL, based on the data of nearby Huzhong weather station from 1974 to 2020, MAAT varied from −5.2 to −2.0°C, with the same climate warming rate as that

https://doi.org/10.5194/essd-2024-187
Preprint. Discussion started: 3 June 2024

of Mo'he (0.3°C/decade); annual precipitation was 272~749 mm, showing an appreciable average wetting rate of 3.1 mm per decade. Precipitation fell concentratively in the form of rain from June to August, accounting for 62%~65% of the annual total. Snow cover generally lasted from October to the next May, with maximum snow depths at 40-50 cm.

The four study areas were selected to observe post-fire changes in permafrost features and soil nutrient conditions (Table 1). This monitoring network includes eight boreholes and soil profiles, and the elements of the observation network for ground temperature, active layer thickness (ALT), soil moisture content (SMC), soil organic carbon (SOC), total nitrogen (TN), total phosphorus (TP), and total potassium (TK). Mean annual ground temperature (MAGT) at the depth of zero annual amplitude (D_{ZAA}, generally at 10-15 m in depth) ranged from –3.25 to –0.56°C, and ALT varied from 1.0 to 3.75 m. The four study areas were all found in the discontinuous permafrost zones, with poor drainage in lowlands and intermontane basins or valleys. Before fires, vegetation was dominated by the Xing'an larch (*Larix gmelinii*) forest, generally with an understory mainly consisting of the shrubs *Ledum palustre* and *Vaccinium uliginosum*, with an organic layer of 55-60 cm in thickness. After fires, the vegetation became gradually dominated by white birch (*Betula platyphylla*) and *Betula fruticosa Pallas*, with an organic layer of 20-45 cm in thickness. The soils in the study area are mainly Histosol and Gelisols (Soil Survey Staff, 2014).

Table 1. Characteristics of the eight study sites for monitoring the thermal state and soil nutrients of the active layer and near-surface permafrost in the northern Da Xing'anling Mountains in Northeast China

Study areas and sites		Lat (°N)	Long. (°E)	Elev. (m a. s. l.)	Veget -ation	Organic layer thickness (cm)	Drainage	Fire severity
MG (Mangui)	MG-S	52.27 65	122.28 91	710	Larch forest	20	Somewhat poor	Severely burned
	MG-U					55	Poor	Unburned
AL	AL-S	51.88	121.90		Larch	25	Moderately	Severely

https://doi.org/10.5194/essd-2024-187
Preprint. Discussion started: 3 June 2024

(Alongshan)	AL-U	68	67	669	forest	55	good Poor	burned Unburned
GL (Gulian)	GL-S GL-U	53.04 32	122.05 04	582	Shrub wetland	30 60	Somewhat poor Poor	Severely burned Unburned
MH (Mo'he)	MH-S MH-U	52.98 59	122.11 15	486	Shrub wetland	30 60	Somewhat poor Poor	Severely burned Unburned

The horizontal distance between MG-U and MG-S was about 200 m, with the MG-U on the edge of the burned area. Observations of ground temperatures began in February 2017 (two years after fire). At MG-U in the Xing'an larch (*Larix gmelinii*) dominated forest, all larch trees at MG-S were burned to death, and low shrubs and herbs were found in 2022. The horizontal distance between AL-U and AL-S was less than 100 m, with the AL-U on the edge of the burned area. Observations of ground temperatures began in February 2017 (eight years after fire). The vegetation was the Xing'an larch forest at AL-U, and; it was the broad-leaved forest (birch) at AL-S. GL-S and GL-U sites were selected about 2 km apart from each other. Measurements of ground temperatures began in February 2017 (15 years after fire). The vegetation was the shrub wetland at GL-U and GL-S. MH-S and MH-U sites were about 5 km apart. Observations of ground temperatures began in February 2017 (30 years after fire). The vegetation was the shrub wetland at MH-U and MH-S.

2.2 Fire severity

Normalized Burn Ratio (NBR) and differential Normalized Burn Ratio (dNBR) are often used to assess the forest fire severity (Cocke et al., 2005; Li et al., 2022b), and the calculation formulas are as follows:

$$NBR = (\rho_{NIR} - \rho_{MIR})/(\rho_{NIR} + \rho_{MIR}) \quad (1)$$

$$dNBR = NBR_{prefire} - NBR_{postfire} \quad (2)$$

where ρ_{NIR} and ρ_{MIR} are the reflectivity values of pixel from the near-infrared (NIR) and middle-infrared (MIR) bands, and; $NBR_{prefire}$ and $NBR_{postfire}$ are the values

https://doi.org/10.5194/essd-2024-187
Preprint. Discussion started: 3 June 2024

of the NBR before and after fire.

According to the values of *dNBR*, fire severity is divided into four categories: severely burned (dNBR $\geqslant$ 0.571), moderately burned (0.241-0.570), lightly burned (0.051-0.240), and unburned ($\leqslant$ 0.050) (Cocke et al., 2005). In the lightly and moderately burned areas, there were difficulties in drilling and/or monitoring due to device malfunction or damage, and thus a lot of data were missing. In addition, the permafrost environment changes more significantly after severe burns. Therefore, only sites of two levels of fire severity (severely burned and unburned) were chosen for the abovementioned four areas (Mangui/MG, Alongshan/AL, Gulian/GL and Mo'he/MH) to study post-fire changes in ground hydrothermal regimes and soil nutrients.

2.3 Site instrumentation and laboratory analysis

At each site of different fire severity, a 20-m-deep borehole was drilled and instrumented in October 2016 to monitor ground temperatures (eight boreholes in total) (Figure 2). Ground temperatures were monitored with 0.5-m depth intervals at depths of 0–5 m and then with 1-m depth intervals at depths of 5–20 m by thermistor cables permanently installed in boreholes and manually measured from February 2017. All thermistors were assembled and calibrated at the Key Laboratory of Cryospheric Science and Frozen Soil Engineering, Northwest Institute of Eco-Environment and Resources (renamed from the merger of the former State Key Laboratory of Frozen Soil Engineering and the State Key Laboratory of Cryosphere Science, Cold and Arid Regions Environmental and Engineering Research Institute), Chinese Academy of Sciences. Since February 2017, ground temperatures at these boreholes were manually measured once a week (Table 2), or occasionally three times per month due to traffic difficulty or control, by a multi-meter Fluke 189® device. According to the measured soil temperatures during the observation period, the isotherms of soil temperature in the vertical profile at depths of 0–20 m were drawn, and then the 0°C isotherms were delineated for each borehole. The values of ALT were then determined, using linear extrapolation of seasonally and progressively changing ground temperature distribution

https://doi.org/10.5194/essd-2024-187
Preprint. Discussion started: 3 June 2024

228 with depth, for each borehole and each year according to the deepest position of the 0˚C
229 isotherms in the year.

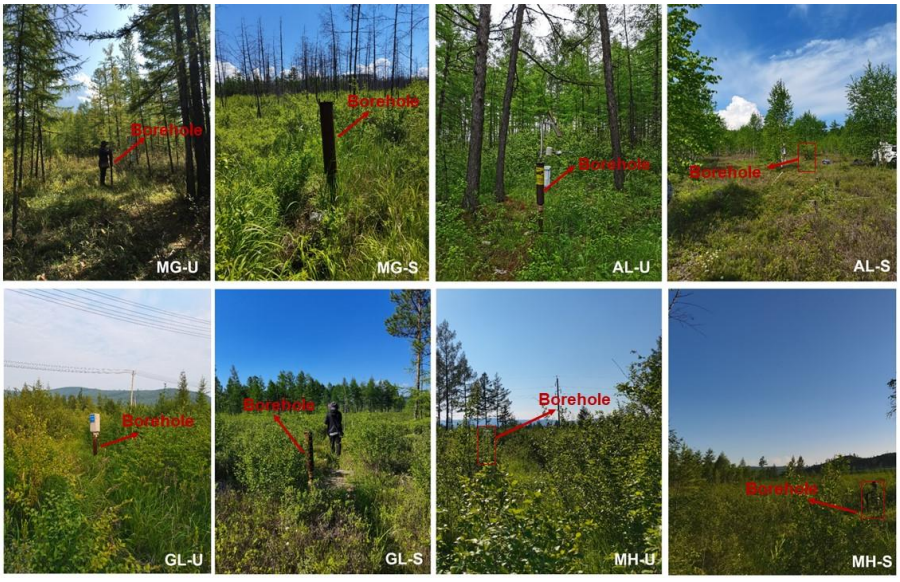

230

231 Figure 2. Photos of the study sites with different vegetation cover and the position of
232 the 20 m deep boreholes for monitoring the ground temperature.

https://doi.org/10.5194/essd-2024-187
Preprint. Discussion started: 3 June 2024

Table 2. Monitoring data for the eight sites of soil nutrients and ground temperature boreholes for studying fire impacts on the permafrost environment in the northern Da Xing'anling Mountains in Northeast China

Study sites	Monitoring depths (m)			Time period	Monitoring frequency
	Soil nutrients	Soil gravimetric moisture content	Ground temperature		
MG-U	0.1, 0.2, 0.3, 0.4, 0.5, 0.6, 0.7, 0.8, 0.9, 1.0, 1.1, 1.2, 1.3, 1.4, 1.5, 1.6, 1.7, 1.8, 1.9, 2.0, 2.1, 2.2, 2.3, 2.4, 2.5	0.2, 0.3, 0.4, 0.5, 0.6, 0.7, 0.8, 0.9, 1.0, 1.1, 1.2, 1.3, 1.4, 1.5, 1.6, 1.7, 2.0, 2.5, 2.7			
MG-S	0.1, 0.2, 0.3, 0.4, 0.5, 0.6, 0.7, 0.8, 0.9, 1.0, 1.1, 1.2, 1.3, 1.4, 1.5, 1.6, 1.7, 1.8, 1.9, 2.0, 2.1, 2.2, 2.3, 2.4, 2.5, 2.6	0.2, 0.3, 0.4, 0.5, 0.6, 0.7, 0.8, 0.9, 1.0, 1.1, 1.2, 1.3, 1.4, 1.5, 1.6, 1.7, 1.8, 1.9, 2.0, 2.1, 2.2, 2.6, 4.6, 5.6, 6.1, 7.6			
AL-U	0.1, 0.2, 0.3, 0.4, 0.5, 0.6, 0.7, 0.8, 0.9, 1.0, 1.1, 1.2, 1.3, 1.4, 1.5, 1.6, 1.7, 1.8, 1.9, 2.0, 2.1, 2.2, 2.3, 2.4, 2.5, 2.6, 2.7, 2.8, 2.9, 3.0	0.1, 0.2, 0.3, 0.4, 0.5, 0.6, 0.7, 0.8, 0.9, 1.0, 1.1, 1.2, 1.3, 1.4, 1.5, 1.6, 1.7, 1.8, 1.9, 2.0, 2.1, 2.2, 2.3, 2.4, 2.5, 2.6, 2.7, 2.8, 2.9, 3.0, 3.1, 3.2, 3.5, 4.0, 4.5, 5.0, 5.5, 5.9, 6.4, 9.4			
AL-S	0.1, 0.2, 0.3, 0.4, 0.5, 0.6, 0.7, 0.8, 0.9, 1.0, 1.1, 1.2, 1.3, 1.4, 2.1, 2.2, 2.3, 2.4, 2.5, 2.6, 2.7, 2.8	0.2, 0.3, 0.4, 0.5, 0.6, 0.7, 0.8, 0.9, 1.1, 1.4, 1.5, 1.7, 2.0, 2.2, 2.4, 2.6, 2.8, 2.9, 3.1, 3.4, 3.6, 4.0, 4.1, 4.5, 4.8, 5.5, 6.0, 7.0, 7.5	0.0, 0.2, 0.5, 1.0, 1.5, 2.0, 2.5, 3.0, 3.5, 4.0, 5.0, 6.0, 7.0, 8.0, 9.0, 10.0, 11, 12, 13, 14, 15, 16, 17, 18, 19, 20	2016; 2016; 2017-2022	Thrice/ month
GL-U	0.1, 0.2, 0.3, 0.4, 0.5, 0.6, 0.7, 0.8, 0.9, 1.0, 1.1, 1.4, 1.5, 1.6, 1.7, 1.8, 1.9, 2.0, 2.1, 2.2, 2.3, 2.4, 2.5, 2.6, 2.7, 2.8, 2.9, 3.0, 3.1, 3.4, 3.5, 3.6	0.1, 0.2, 0.3, 0.4, 0.5, 0.6, 0.7, 0.8, 0.9, 1.0, 1.1, 1.3, 1.4, 1.5, 1.6, 1.7, 1.8, 1.9, 2.0, 2.7, 2.8, 2.9, 3.0, 3.1			
GL-S	0.1, 0.2, 0.3, 0.4, 0.5, 0.6, 0.7, 0.8, 0.9, 1.0, 1.2, 1.3, 1.4, 1.5, 2.0, 2.1, 2.2, 2.4, 2.5, 2.6, 2.7, 2.8	0.1, 0.2, 0.3, 0.8, 2.0, 2.4, 2.7, 3.6, 4.2, 4.7, 5.6, 8.4			
MH-U	0.1, 0.2, 0.3, 0.4, 0.5, 0.6, 0.7, 0.8, 0.9, 1.0, 1.1, 1.4, 1.5, 1.6, 1.7, 1.8, 1.9, 2.0, 2.1, 2.2, 2.3, 2.4, 2.5, 2.6, 2.7, 2.8, 2.9, 3.0, 3.1, 3.4, 3.5, 3.6	0.1, 0.2, 0.3, 0.4, 0.5, 0.6, 0.7, 0.8, 0.9, 1.0, 1.1, 1.3, 1.4, 1.5, 1.6, 1.7, 1.8, 1.9, 2.0, 2.7, 2.8, 2.9, 3.0, 3.1			
MH-S	0.1, 0.2, 0.3, 0.4, 0.5, 0.6, 0.7, 0.8, 0.9, 1.0, 1.1, 1.2, 1.3, 1.4, 1.5, 1.6, 1.7, 1.8, 1.9, 2.0	0.1, 0.2, 0.3, 0.4, 0.5, 0.6, 0.7, 0.8, 0.9, 1.0, 1.1, 1.2, 1.3, 1.4, 1.5, 1.6, 1.7, 1.8, 1.9, 2.0, 2.3, 3.6			

https://doi.org/10.5194/essd-2024-187
Preprint. Discussion started: 3 June 2024

While drilling in 2016, soil samples were collected from depths of 0-9.4 m at intervals of 0.1-3.0 m, with a total of 402 soil samples. At depths of 0-3.0 m, samples were collected every 10 cm in depth in soil strata with more complex changes near the ground surface. At depths of 3.0-9.4 m, samples were collected based on lithological similarity or changes in soil or rock strata, rather than at an equal depth interval of 0.1 m. Therefore, at depths of 0-3 m, there was generally a set of data at a regular depth interval of 10 cm, but at depths of 3-10 m, the depth intervals of datasets varied substantially. One part of the soil samples was collected using a cutting ring and stored in an 100-cm^3 aluminum specimen box and immediately weighed (soil wet weight). Then, the samples were transported to the laboratory and dried at 105°C to obtain soil dry weight. Finally, gravimetrically-based SMC was calculated by the mass of soil before and after drying. The other part of the soil samples was collected and stored in zip-lock bags and timely brought back to the laboratory for air-drying, then passed through a 2-mm sieve for chemical analysis. SOC and TN contents were measured by potassium dichromate oxidation reduction and Kjeldahl nitrate boiling fluid injection methods, respectively (Nelson et al., 1982). TP and TK contents were determined by the methods of Mo-Sb colorimetry and flame photometry, respectively (Sun et al., 2011). These data are shown as mean ± standard error (SE). Changes in ground temperatures and soil chemical properties were analyzed using the space-for-time chronosequence approach (Mack et al., 2021).

2.4 Data quality check

The measurement accuracy of ground temperature was ±0.05°C in the range of −30 to +30°C, but ± 0.1°C in those of −45 to −30°C and +30 to +50°C. From 2020 to 2022, due to the breakout and persistence of the COVID-19 epidemic, some data were not timely measured, affecting the sampling intervals. Ground temperature data were collected manually three times a month since February 2017, and after the outbreak of the COVID-19 epidemic, the data were recorded once or twice a month. In addition, some data were missing because of damaged, broken, or destroyed probes, solar panel batteries, or dataloggers. From 6 February 2017 to 22 November 2022, a total of 28,890

https://doi.org/10.5194/essd-2024-187
Preprint. Discussion started: 3 June 2024

pieces of data were collected, of which 178 NA (not available) data were resulted from probe damage, thus 28,712 valid data were collected. All the missing data were near the ground surface, at a soil layer at depths between 0 and 5 cm. At MG-U, AL-U, AL-S, GL-S, and MH-S, all the data were available. Of the 178 NA data, 74 were at MG-S (from 17 September 2019 to 22 November 2022), 52 at GL-U (from 20 July 2019 to 13 February 2022), and 52 at MH-U (from 20 July 2019 to 13 February 2022) sites. Data of soil temperatures from manually monitored boreholes were quality-controlled for each measurement. Some studies have also shown that this method of monitoring ground temperature using drilling and probes is one of the most accurate, reliable, and intuitive methods for long-term monitoring of permafrost data (Chang et al., 2022; Li et al., 2022a, 2024; Zhao et al., 2021). Before the analysis of soil nutrient data and SMC data, we conducted outlier tests to ensure the accuracy of the data. These tests showed that all the data have no outliers and the samples are representative. There was a total of 840 soil nutrient data and 195 SMC data.

3 Data descriptions and evaluation

3.1 Changes in ground temperatures of near-surface permafrost

Ground temperatures at depths of 0-20 m in the active layer and near-surface permafrost showed remarkable seasonal dynamics (Figures 3 and 4). The amplitudes of changes in ground temperature decreased exponentially with increasing depth. At depths of 0-1 m, the changes in MAGT at eight sites were larger 1.5-10.2℃ than those at 1-20 m (Figure 3a to 3d).

https://doi.org/10.5194/essd-2024-187
Preprint. Discussion started: 3 June 2024

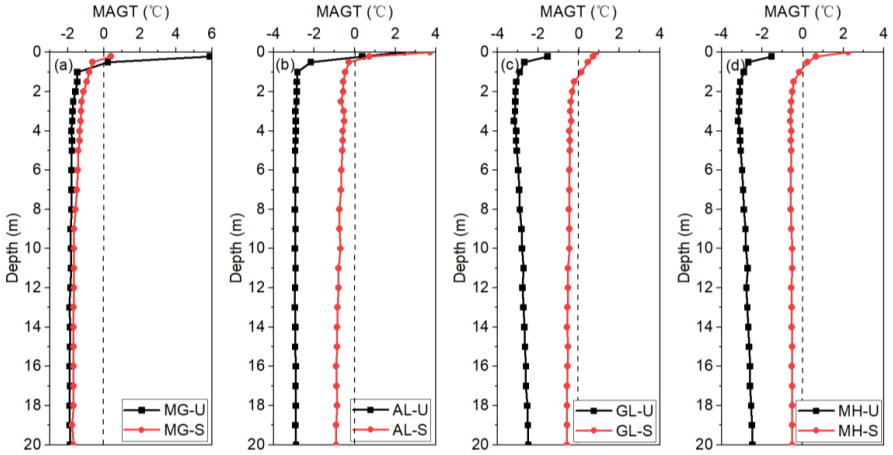

Figure 3. Mean annual ground temperatures (MAGTs) from 2017 to 2022 at the unburned and severely burned sites in the four areas on the western flank of the northern Da Xing'anling Mountains in Northeast China

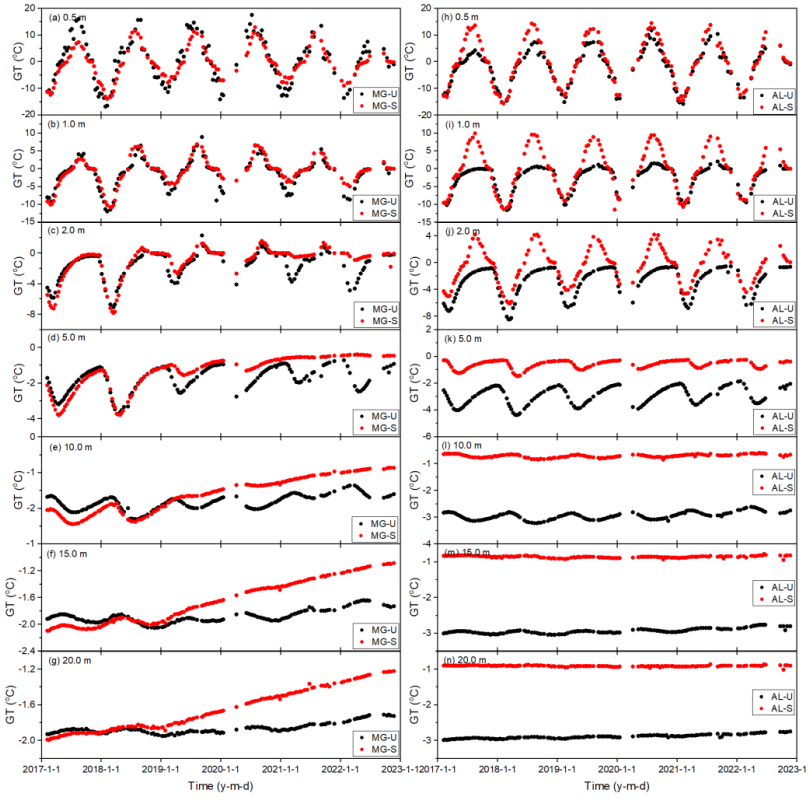

Figure 4. Variability of ground temperatures at depths of 0–20 m at Xing'an larch forest sites in Mangui (MG) and Alongshan (AL) on the western flank of the northern Da Xing'anling Mountains in Northeast China during the period from 2017 to 2022.

https://doi.org/10.5194/essd-2024-187
Preprint. Discussion started: 3 June 2024

Notes: The symbol U stands for the unburned site, S for the severely burned site, and; GT, for ground temperature.

The MAGTs lowered with increasing depths, the temperature difference between 0.5 m and 20 m was 0.2-2.1℃ (Table 3). From 2017 to 2022, ground temperature fluctuated in a sinusoidal pattern at depths of 0.5 to 2.0 m, and this dynamic change gradually disappeared with increasing depth (Figures 3a to 3g and 5a to 5g). At a depth of 5 m, ground temperature was subzero perennially (Figures 4d, 4k, 5d, and 5k). At eight sites, from 2017 to 2022, ground temperatures showed an increasing trend at depths of 0.5-20 m, with increase rates of 0.01-0.69℃/yr. The increase rate was the largest at AL-U (0.03-0.69℃/yr), and; the lowest, at AL-S and GL-S (all were 0.01-0.37℃/yr) (Figures 4a to 4g and Figures 5a to 5g).

Table 3. Mean annual ground temperatures (MAGTs) at each of the seven measured depths of the unburned and severely burned sites in the four areas on the western flank of the northern Da Xing'anling Mountains in Northeast China during the period from 2017 to 2022

Depths	0.5 m		1.0 m		2.0 m		5.0 m		10 m		15 m		20 m	
Fire	U	S	U	S	U	S	U	S	U	S	U	S	U	S
MG	0.2	-0.6	-1.5	-0.8	-1.6	-1.1	-1.7	-1.4	-1.8	-1.6	-1.9	-1.7	-1.9	-1.7
AL	-2.2	-0.3	-2.8	-0.5	-2.9	-0.6	-2.9	-0.6	-2.9	-0.7	-2.9	-0.9	-2.9	-0.9
GL	-2.7	0.5	-2.9	0.1	-3.1	-0.3	-3.1	-0.4	-2.8	-0.5	-2.6	-0.5	-2.5	-0.6
MH	-2.7	0.2	-2.9	-0.2	-3.1	-0.5	-3.1	-0.6	-2.8	-0.5	-2.6	-0.5	-2.5	-0.5

Notes: U stands for the unburned sites, and S, the severely burned sites.

https://doi.org/10.5194/essd-2024-187
Preprint. Discussion started: 3 June 2024

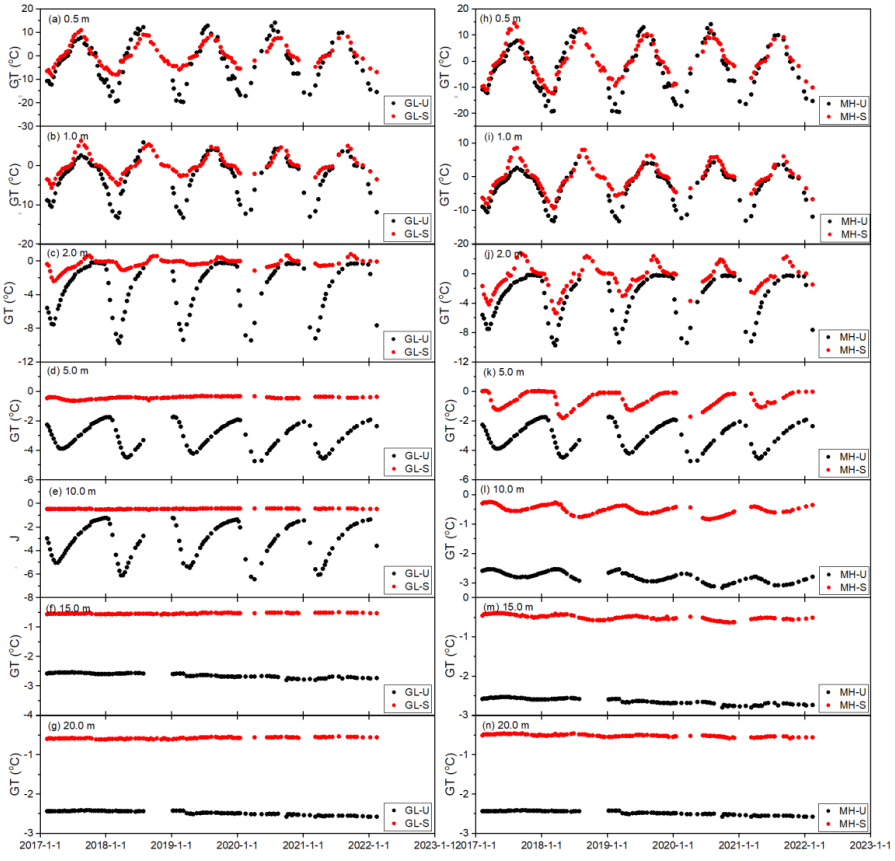

Figure 5. Variations in ground temperatures at depths of 0–20 m at shrub wetlands sites in Gulian (GL) and Mo'he (MH) on the western flank of the northern Da Xing'anling Mountains in Northeast China during the period from 2017 to 2022. Notes: The symbol U stands for the unburned site; S, for the severely burned site, and; GT, for ground temperature.

3.2 Changes in MAGTs at the permafrost table ($MAGT_{PT}$) and D_{ZAA} ($MAGT_{DZAA}$)

MAGTs at the permafrost table ($MAGT_{PT}$) and at the D_{ZAA} ($MAGT_{DZAA}$) can truly reflect the changing characteristics of permafrost thermal regimes. Therefore, in this section, we choose $MAGT_{PT}$ and $MAGT_{DZAA}$ to briefly analyze changes in ground thermal regimes. When the temperature probe was missing at the actual depth of the permafrost table or the D_{ZAA}, $MAGT_{PT}$ and $MAGT_{DZAA}$ were derived from interpolation of adjacent ground temperatures.

https://doi.org/10.5194/essd-2024-187
Preprint. Discussion started: 3 June 2024

In the eight monitored sites, the permafrost table ranged between 1.5 and 4.5 m, and the D_{ZAA} between 10 and 16 m. From 2017 to 2022, except for GL-U, MH-U and MH-S sites, $MAGT_{PT}$ and $MAGT_{DZAA}$ decreased gradually (-0.02–-0.06℃/yr), while at other sites increased at rates of 0.01- 0.54℃/yr (Figure 6). The ground warming rates of $MAGT_{PT}$ and $MAGT_{DAZZ}$ were highest at the MG-S site (both at 0.54℃/yr), and lowest at the GL-S site (0.10 and 0.01℃/yr) (Figures 6a and 6b). From 2017-2022, the highest differences in $MAGT_{PT}$ and $MAGT_{DAZZ}$ were 2.6 and 1.3℃ at the MG-S site, respectively, and the lowest were 0.2 and 0.1℃ at MH-S and AL-S sites, respectively (Figures 6a, 6d and 6h).

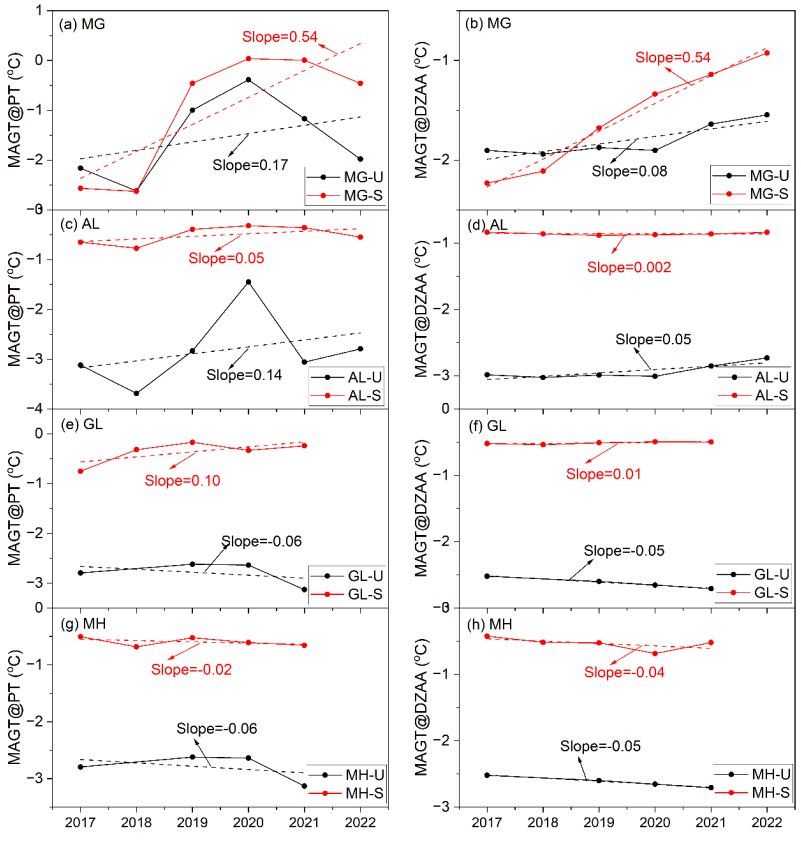

Figure 6. Variations in mean annual ground temperatures at the permafrost table ($MAGT_{PT}$) and the depth of zero annual amplitude (D_{ZAA}) ($MAGT_{DZAA}$) at eight sites in the four study areas (Mangui/MG, Alongshan/AL, Gulian/GL, and Mo'he/MH) on the western flank of the northern Da Xing'anling Mountains in Northeast China during 2017-2022.

Notes: The symbol U stands for the unburned site, and S, for the severely burned site.

https://doi.org/10.5194/essd-2024-187
Preprint. Discussion started: 3 June 2024

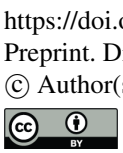

3.3 Active layer thickness (ALT) data

ALT, *i.e.*, the annual maximum depth of seasonal thaw penetration, was determined according to the deepest position of the 0°C isotherms in a year. Although some data were missing, the change trends of ALT were still obvious (Figure 7).

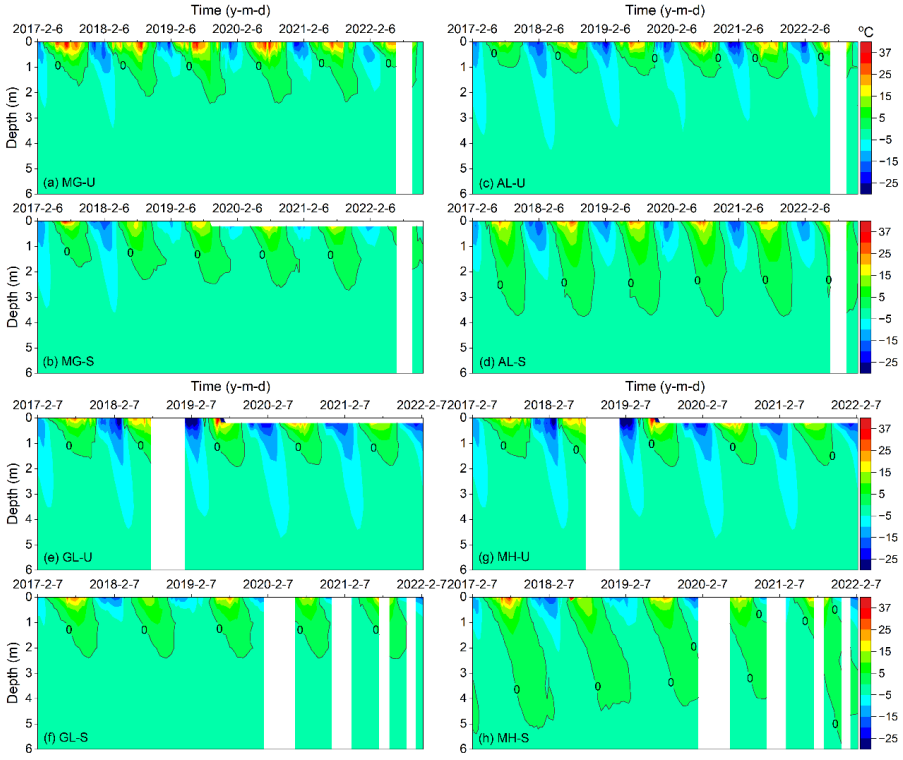

Figure 7. Variability of ground temperatures isotherms at eight sites in Mangui (MG), Alongshan (AL), Gulian (GL), and Mo'he (MH) on the western flank of the northern Da Xing'anling Mountains in Northeast China during 2017-2022.

Notes: U stands for the unburned sites, as in insets a (site MG-U), c (site AL-U), e (site GL-U), and g (site MH-U), and S, the severely burned sites, as in insets b (site MG-S), d (site AL-S), f (site GL-S), and h (site MH-S).

ALT was between 1.0 and 5.2 m at the eight sites from 2017 to 2022, and the maximum average of ALT was 4.5 m at MH-U and the minimum was 1.6 m at AL-U. Compared with the other seven sites, MH-S has the largest ALT, with a maximum value

https://doi.org/10.5194/essd-2024-187
Preprint. Discussion started: 3 June 2024

of 5.2 m in 2017. From 2017 and 2022, only at the MH-S site, ALT decreased at a rate of 36.5 cm/yr, while at the other sites it increased at rates of 0.1-20.5 cm/yr. The increase rate of ALT at MG-S was the fastest, and; at AL-S, the slowest (Figure 8).

Figure 8. Variation characteristics of active layer thickness (ALT) from 2017 to 2022 at eight sites of the four study areas in Mangui (MG), Alongshan (AL), Gulian (GL), and Mo'he (MH) on the western flank of the northern Da Xing'anling Mountains in Northeast China during 2017-2022. Notes: U stands for the unburned site, and S, the severely burned site.

3.4 Variations in gravimetric soil moisture content (SMC)

At MG-U and AL-U sites, SMC decreased with increasing depth, especially in the active layer and near-surface permafrost, or in the vicinity of the permafrost table (Figure 9). For example, at AL-U, SMC decreased at a rate of 8.6%/m and average SMC was 108.2±11.7% at depths of 0-9.4 m (Figure 9b). At the depths (0-3 m) with higher SMC, the soil contains massive ice crystals and a large amount of segregated ice, with ice lenses of 0.1–5.0 cm thickness. Such as at GL-U, the SMC was higher at the

https://doi.org/10.5194/essd-2024-187
Preprint. Discussion started: 3 June 2024

junction of the active layer bottom and upper layer of transient permafrost (1-2 m in depth) due to a large amount of segregated ice (0.2-5.0 cm thick) under the permafrost table. At MG-S, AL-S, GL-S, and MH-S sites, changes in SMC were inconspicuous, only at depths of 0-0.5 m, SMC showed a slight decreasing trend. At depths of 0.5-9.4 m, differences in SMC were minor (Figure 9). At MG-S, SMC fluctuated between 11.7-63.2% at depths of 0.6-7.6 m, with average SMC at 27.5±3.2% (Figure 9a). At AL-S, GL-S, and MH-S sites, SMC fluctuated between 4.7-26.6% at depths of 0.6-8.4 m, with average SMC of 17.1-21.1%.

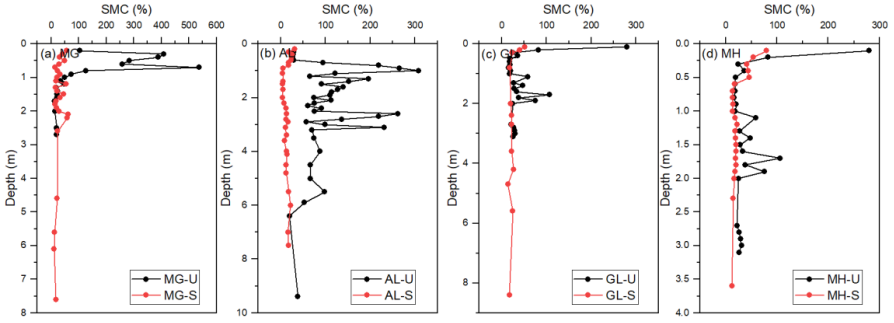

Figure 9. Variations in gravimetrically-based soil moisture contents (SMC) with different fire severity at eight sites in Mangui (MG), Alongshan (AL), Gulian (GL), and Mo'he (MH) on the western flank of the northern Da Xing'anling Mountains in Northeast China in 2016. Notes: The symbol U stands for unburned, S for severely burned, and; SMC, for soil gravimetric moisture content.

3.5 Variations in soil nutrients

The contents of SOC and TN decreased with increasing depths. A large amount of SOC and TN were stored in the active layer (0-1.3 m), especially in the soil organic layer (0-0.5 m) (Figures 10a to 10n). The change trends of SOC and TN were consistent. For example, at MG-U, at depths of 0-1.3 m, averages of SOC and TN were 140.5±26.9 and 5.9±0.9 g/kg, respectively; at depths of 1.3-2.5 m, changes in SOC and TN were relatively smooth, fluctuating between 2.0-13.3 and 0.9-1.5 g/kg, with averages at 5.4±1.1 and 1.2±0.1 g/kg, respectively (Figures 10a and 10b).

https://doi.org/10.5194/essd-2024-187
Preprint. Discussion started: 3 June 2024

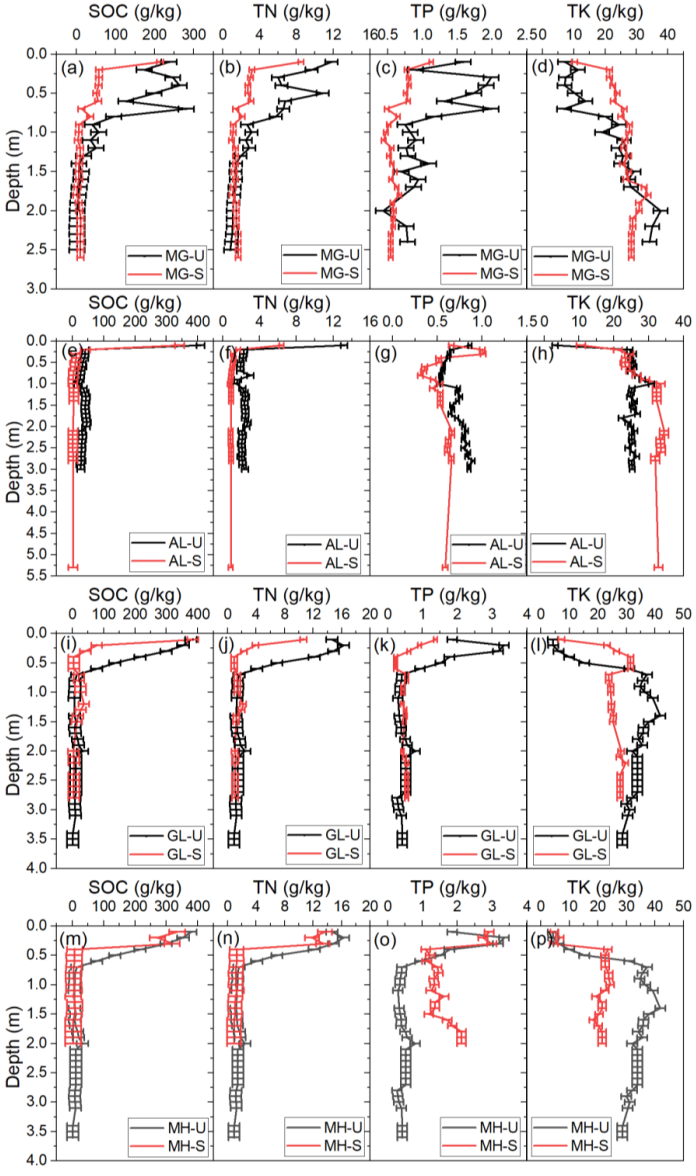

Figure 10. Variations in soil nutrients at eight sites in Mangui (MG, a to d), Alongshan (AL, e to h), Gulian (GL, i to l), and Mo'he (MH, m to p) on the western flank of the northern Da Xing'anling Mountains in Northeast China in 2016. Notes:

1) The symbol U stands for unburned, and S for severely burned.

2) SOC stands for soil organic carbon; TN, for total nitrogen; TP, for total phosphorus, and; TK, for total potassium.

https://doi.org/10.5194/essd-2024-187
Preprint. Discussion started: 3 June 2024

TP contents decreased up to 1.0 m in depth, and changes in TP were minor at depths of 1.0-5.3 m (Figures 10c, 10g, 10k, and 10o). For example, at MG-S, TP decreased at a rate of 0.56 g/kg/m at depths of 0-1.0 m, with an average of 0.7±0.1 g/kg (Figure 10c); TP fluctuated between 0.4 and 0.7 g/kg at depths of 1.1-2.6 m, with an average of 0.6±0.01 g/kg. The change trends of TK were opposite with TP because TK contents increased downwards (Figures 10d, 10h, 10l, and 10p). The contents of TK were all below 41.8 g/kg. For example, at MG-U, TK increased at a rate of 14.1 g/kg/m, while TP decreased at a rate of 0.5 g/kg/m (Figures 10c and 10d).

4. Data availability

The dataset of ground temperature, ALT, SMC, SOC, and contents of TN, TP, and TK can be freely downloaded and is available from the National Tibetan Plateau/Third Pole Environment Data Center (https://doi.org/10.11888/Cryos.tpdc.300933, Li and Jin, 2024). The dataset was classified into three categories: ground temperatures (at MG-U, MG-S, AL-U, AL-S, GL-U, GL-S, MH-U, and MH-S), soil moisture contents (SMCs), and soil nutrient contents (SOC, TN, TP, and TK).

5. Conclusions

The Da Xing'anling (Hinggan) Mountains in Northeast China are located on the southern margin of the Eastern Asia permafrost zone and boreal forest belt. It is an area where fires occur frequently and the thermal state of permafrost is sensitive to fire disturbances. To study fire effects on the permafrost environment, a monitoring network has been established in Northeast China since 2016. Therefore, a long-term field dataset on ground hydrothermal regimes and soil nutrients has been obtained. This dataset fills a gap in a long-term monitoring study of fire effects on the permafrost environment in the hemiboreal forest zone in Northeast China. These data included ground temperatures at depths of 0-20 m, SMC at depths of 0-9.4 m, and contents of SOC, TN, TP, and TK at depths of 0-3.6 m. The data were collected from eight sites from 2016 to 2022 in four burned areas (MG in Mangui, AL in Alongshan, GL in Gulian, and MH in Mo'he) with two categories of fire severity (severely burned and unburned).

Long-term monitoring data in the northern Da Xing'anling Mountains in Northeast

https://doi.org/10.5194/essd-2024-187
Preprint. Discussion started: 3 June 2024

China have shown a degrading permafrost under the disturbances of climate change and frequent forest fires. This is evidenced by increasing ground temperature, thickening active layer, decreasing SMC, and evident changes in soil nutrient contents. The 6-year long-term dataset presented in this study has a high-quality time series with only a few missing data. This valuable and hard-won dataset of forest fires and permafrost is worth maintaining and improving in the future. This study provides important basic data for the protection of the ecosystem-dominated Xing'an permafrost and herewith boreal permafrost ecosystems. Furthermore, it is useful for more accurate prediction of fire-induced permafrost changes and for more accurate estimating and better-managing soil carbon stocks. It also provides an important reference for the initiatives of carbon neutralization and carbon peaking control and the assessment of infrastructure safety under fire threats.

Author contributions. XL and HJ designed and conducted this research. XL compiled the dataset, performed the data analysis, and wrote the manuscript. RH, HW, XC, RȘ, and ZT participated in the fieldwork. HJ, QF, QW, DL and RȘ improved the writing. XL prepared the manuscript with contributions from all co-authors.

Competing interests. The authors declare that they have no conflict of interest.

Disclaimer. Publisher's note: Copernicus Publications remains neutral with regard to jurisdictional claims in published maps and institutional affiliations.

Acknowledgments. We would like to thank all the scientists and students who participated in the fieldwork. We thank the two anonymous reviewers for their thorough reviews and insightful comments that improved the paper. We also are grateful to Professor Xin Li for his encouragement, guidelines, and review of the proposal for writing up this paper and preparation of the datasets.

Financial support. This research has been supported by the National Natural Science Foundation of China (Grant No. 32241032); Heilongjiang Excellent Youth Fund (Grant No. YQ2022D002), and; Fundamental Research Fund for the Central Universities (Grant Nos. 2572023CT01 and 2572021GT08). Raul-David Șerban

https://doi.org/10.5194/essd-2024-187
Preprint. Discussion started: 3 June 2024

received funding from the Autonomous Province of Bozen/Bolzano-Department for Innovation, Research and University (Grant No. 13585/2023).

References

Ackley, C., Tank, S. E., Haynes, K. M., Rezanezhad, F., McCarter, C. and Quinton, W. L.: Coupled hydrological and geochemical impacts of wildfire in peatland-dominated regions of discontinuous permafrost, Sci. Total Environ., 782, 146841, https://doi.org/10.1016/j.scitotenv.2021.146841, 2021.

Balser, A. W., Jones, J. B. and Gens, R.: Timing of retrogressive thaw slump initiation in the Noatak Basin, northwest Alaska, USA, J. Geophys. Res.-Earth Surf., 119, 1106-1120, https://doi.org/10.1002/2013JF002889, 2014.

Biskaborn, B. K., Smith, S. L., Noetzli, J., Matthes, H., Vieira, G., Streletskiy, D. A., Schoeneich, P., Romanovsky, V. E., Lewkowicz, A. G., Abramov, A., Allard, M., Boike, J., Cable, W. L., Christiansen, H. H., Delaloye, R., Diekmann, B., Drozdov, D., Etzelmuller, B., Grosse, G., Guglielmin, M., Ingeman-Nielsen, T., Isaksen, K., Ishikawa, M., Johansson, M., Johannsson, H., Joo, A., Kaverin, D., Kholodov, A., Konstantinov, P., Kroger, T., Lambiel, C., Lanckman, J. P., Luo, D., Malkova, G., Meiklejohn, I., Moskalenko, N., Oliva, M., Phillips, M., Ramos, M., Sannel, A. B. K., Sergeev, D., Seybold, C., Skryabin, P., Vasiliev, A., Wu, Q., Yoshikawa, K., Zheleznyak, M. and Lantuit, H.: Permafrost is warming at a global scale, Nat. Commun., 10, 264, doi: 10.1038/s41467-018-08240-4, 2019.

Boyd, M. A., Walker, X. J., Barnes, J., Celis, G., Goetz, S. J., Johnstone, J. F., Link, N. T., Melvin, A. M., Saperstein, L., Schuur, E. A. G. and Mack, M. C.: Decadal impacts of wildfire fuel reduction treatments on ecosystem characteristics and fire behavior in Alaskan boreal forests, For. Ecol. Manage., 546, 121347, doi: 10.1016/j.foreco.2023.121347, 2023.

Brown, D. R. N., Jorgenson, M. T., Douglas, T. A., Romanovsky, V. E., Kielland, K., Hiemstra, C., Euskirchen, E. S. and Ruess, R. W.: Interactive effects of wildfire and climate on permafrost degradation in Alaskan lowland forests, J. Geophys. Res.-Biogeosci., 120, 1619-1637, doi: 10.1002/2015jg003033, 2015.

Chang, X., Jin, H., Zhang, Y., Li, X., He, R., Li, Y., Lü, L. and Wang, H.: Permafrost thermal dynamics at a local scale in northern Da Xing'anling Mountains. Environ. Res. Lett., 19(6), 064014. doi: 10.1088/1748-9326/ad42b6, 2024.

Chang, X., Jin, H., He, R., Zhang, Y., Li, X., Jin, X. and Li, G.: Permafrost changes in the northwestern Da Xing'anling Mountains, Northeast China, in the past decade, Earth Syst. Sci. Data, 14, 3947-3959, doi: 10.5194/essd-14-3947-2022, 2022.

Chen, X., Kang, S., Hu, Y. and Yang, J.: Temporal and spatial analysis of vegetation fire activity in the circum-Arctic during 2001–2020. Res. Cold Arid Reg., 15(1), 48-56, https://doi.org/10.1016/j.rcar.2023.03.002, 2023.

Chen, Y., Kelly, R., Genet, H., Lara, M. J., Chipman, M. L., McGuire, A. D. and Hu, F. S.: Resilience and sensitivity of ecosystem carbon stocks to fire-regime change in Alaskan tundra, Sci. Total Environ., 806, 151482, doi: 10.1016/j.scitotenv.2021.151482, 2022.

Chen, Y., Hu, F. and Lara, M. J.: Divergent shrub-cover responses driven by climate, wildfire, and permafrost interactions in Arctic tundra ecosystems, Glob. Change Biol., 27, 652-663, 2021.

Cocke, A. E., Fulé, P. Z. and Crouse, J. E.: Comparison of burn severity assessments using Differenced Normalized Burn Ratio and ground data, Int. J. Wildl. Fire, 14, 189-198, 2005.

https://doi.org/10.5194/essd-2024-187
Preprint. Discussion started: 3 June 2024

493 Fedorov, N. A. and Basharin, N. I.: Activation of thermokarst after forest fires on the Yansky plateau: the
494 case of Verkhoyansk area (in Russian), Bull. NEFU. Ser. “Earth Sci.”, 1, 46-57,
495 doi: 10.25587/SVFU.2022.25.1.013, 2022.
496 French, N. H. F., Jenkins, L. K., Loboda, T. V., Flannigan, M., Jandt, R., Bourgeau-Chavez, L. L. and
497 Whitley, M.: Fire in arctic tundra of Alaska: past fire activity, future fire potential, and significance
498 for land management and ecology, Int. J. Wildl. Fire, 24, 1045-1061, 2015.
499 Fultz, L. M., Moore-Kucera, J., Dathe, J., Davinic, M., Perry, G., Wester, D., Schwilk, D. W. and Rideout-
500 Hanzak, S.: Forest wildfire and grassland prescribed fire effects on soil biogeochemical processes
501 and microbial communities: Two case studies in the semi-arid Southwest, Appl. Soil Ecol., 99, 118-
502 128, doi: 10.1016/j.apsoil.2015.10.023, 2016.
503 Gruber, S. and Haeberli, W.: Permafrost in steep bedrock slopes and its temperature-related
504 destabilization following climate change, J. Geophys. Res.-Earth Surf., 112, F02S18, doi:
505 10.1029/2006JF000547, 2007.
506 Jin, H., Li, S., Cheng, G., Wang, S. and Li, X.: Permafrost and climatic change in China, Glob. Planet
507 Chan., 26, 387-404, doi: 10.1016/S0921-8181(00)00051-5, 2000.
508 Jin, H., Yu, Q., Lü, L., Guo, D., He, R., Yu, S., Sun, G. and Li, Y.: Degradation of permafrost in the
509 Xing'anling Mountains, northeastern China, Permafr. Periglac. Process., 18, 245-258, doi:
510 10.1002/ppp.589, 2007.
511 Jin, H., Wu, Q. and Romanovsky, V.E.: Editorial: Impacts from degrading permafrost, Adv. Clim. Change
512 Res., 12(1), 1-5. doi: 10.1016/j.accre.2021.01.007, 2021.
513 Jin, H., Huang, Y., Bense, V. F., Ma, Q., Marchenko, S. S., Shepelev, V. V., Hu, Y., Liang, S., Spektor, V.
514 V., Jin, X., Li, X. and Li X.: Permafrost degradation and its hydrogeological impacts, Water, 14(3),
515 372. doi: 10.3390/w14030372, 2022.
516 Jin, H., Yang, D., Makarieva, O. and Tang, L.: Changes in permafrost and snow cover in the Boreal and
517 Arctic zones (BAZ) and their impacts, Adv. Clim. Change Res., 14(2), 157-163. doi:
518 10.1016/j.accre.2023.04.002, 2023.
519 Johnstone, J. F., Chapin Iii, F. S., Foote, J., Kemmett, S., Price, K. and Viereck, L.: Decadal observations
520 of tree regeneration following fire in boreal forests, Can. J. For. Res., 34, 267-273, doi: 10.1139/x03-
521 183, 2004.
522 Johnstone, J. F., Hollingsworth, T. N., Chapin Iii, F. S. and Mack, M. C.: Changes in fire regime break
523 the legacy lock on successional trajectories in Alaskan boreal forest, Glob. Change Biol., 16, 1281-
524 1295, doi: 10.1111/j.1365-2486.2009.02051.x, 2010.
525 Jones, B. M., Grosse, G., Arp, C. D., Miller, E., Liu, L., Hayes, D. J. and Larsen, C. F.: Recent Arctic
526 tundra fire initiates widespread thermokarst development, Sci. Rep., 5, 15865, doi:
527 10.1038/srep15865, 2015.
528 Jorgenson, M. T., Harden, J., Kanevskiy, M., O'Donnell, J., Wickland, K., Ewing, S., Manies, K., Zhuang,
529 Q. L., Shur, Y., Striegl, R. and Koch, J.: Reorganization of vegetation, hydrology and soil carbon
530 after permafrost degradation across heterogeneous boreal landscapes, Environ. Res. Lett., 8, 035017,
531 doi: 10.1088/1748-9326/8/3/035017, 2013.
532 Knorr, W., Arneth, A. and Jiang, L.: Demographic controls of future global fire risk, Nat. Clim. Change,
533 6, 781-785, doi: 10.1038/nclimate2999, 2016.
534 Kokelj, S. V. and Jorgenson, M. T.: Advances in thermokarst research, Permafr. Periglac. Process., 24,
535 108-119, doi: 10.1002/ppp.1779, 2013.
536 Kokelj, S. V., Lantz, T. C., Kanigan, J., Smith, S. L. and Coutts, R.: Origin and polycyclic behaviour of

https://doi.org/10.5194/essd-2024-187
Preprint. Discussion started: 3 June 2024

tundra thaw slumps, Mackenzie Delta region, Northwest Territories, Canada, Permafr. Periglac. Process., 20, 173-184, doi: 10.1002/ppp.642, 2009.

Kopp, B. J., Lange, J. and Menzel, L.: Effects of wildfire on runoff generating processes in northern Mongolia, Reg. Envir. Change, 17, 1951-1963, doi: 10.1007/s10113-016-0962-y, 2017.

Koven, C. D., Schuur, E. A. G., Schädel, C., Bohn, T. J., Burke, E. J., Chen, G., Chen, X., Ciais, P., Grosse, G., Harden, J. W., Hayes, D. J., Hugelius, G., Jafarov, E. E., Krinner, G., Kuhry, P., Lawrence, D. M., MacDougall, A. H., Marchenko, S. S., McGuire, A. D., Natali, S. M., Nicolsky, D. J., Olefeldt, D., Peng, S., Romanovsky, V. E., Schaefer, K. M., Strauss, J., Treat, C. C. and Turetsky, M.: A simplified, data-constrained approach to estimate the permafrost carbon–climate feedback, Philos. Trans. R. Soc. Lond. Ser. A-Math. Phys. Eng. Sci., 373, 20140423, doi: 10.1098/rsta.2014.0423, 2015.

Lewkowicz, A. G. and Harris, C.: Frequency and magnitude of active-layer detachment failures in discontinuous and continuous permafrost, northern Canada, Permafr. Periglac. Process., 16, 115-130, doi: 10.1002/ppp.522, 2005.

Lewkowicz, A. G., Etzelmüller, B. and Smith, S. L.: Characteristics of discontinuous permafrost based on ground temperature measurements and electrical resistivity tomography, southern Yukon, Canada, Permafr. Periglac. Process., 22, 320-342, doi: 10.1002/ppp.703, 2011.

Li, G., Ma, W., Wang, F., Jin, H., Fedorov, A., Chen, D., Wu, G., Cao, Y., Zhou, Y., Mu, Y., Mao, Y., Zhang, J., Gao, K., Jin, X., He, R., Li, X. and Li, Y.: A newly integrated ground temperature dataset of permafrost along the China–Russia crude oil pipeline route in Northeast China, Earth Syst. Sci. Data, 14, 5093-5110, doi: 10.5194/essd-14-5093-2022, 2022a.

Li, X. and Jin, H.: An integrated dataset of ground hydrothermal regimes and soil nutrients monitored during 2016-2022 in burned areas in Northeast China. National Tibetan Plateau/Third Pole Environment Data Center. doi: 10.11888/Cryos.tpdc.300933, 2024.

Li, X., Jin, H., He, R., Wang, H., Sun, L., Luo, D., Huang, Y., Li, Y., Chang, X., Wang, L. and Wei, C.: Impact of wildfire on soil carbon and nitrogen storage and vegetation succession in the Nanweng'he National Natural Wetlands Reserve, Northeast China, Catena, 221, 106797, doi: 10.1016/j.catena.2022.106797, 2023.

Li, X., Jin, H., He, R., Huang, Y., Wang, H., Luo, D., Jin, X., Lu, L., Wang, L., Li, W., Wei, C., Chang, X., Yang, S. and Yu, S.: Effects of forest fires on the permafrost environment in the northern Da Xing'anling (Hinggan) mountains, Northeast China, Permafr. Periglac. Process., 30, 163-177, 2019.

Li, X., Jin, H., Wang, H., Jin, X., Bense, V. F., Marchenko, S. S., He, R., Huang, Y. and Luo, D.: Effects of fire history on thermal regimes of permafrost in the northern Da Xing'anling Mountains, NE China, Geoderma, 410, 115670, doi: 10.1016/j.geoderma.2021.115670, 2022b.

Li, X., Jin, H., Sun, L., Wang, H., Huang, Y., He, R., Chang, X., Yu, S. and Zang, S.: TTOP-model-based maps of permafrost distribution in Northeast China for 1961–2020, Permafr. Periglac. Process., 33, 425-435, doi: 10.1002/ppp.2157, 2022c.

Li, X., Jin, H., Wang, H., Marchenko, S. S., Shan, W., Luo, D., He, R., Spektor, V., Huang, Y., Li, X. and Jia, N.: Influences of forest fires on the permafrost environment: A review, Adv. Clim. Change Res., 12, 48-65, 2021.

Liang, L., Zhou, Y., Wang, J. and Gao, X.: Changes to the permafrost environment after forest fire, Da Xi'an Ridge, Gulian mining area, China (in Chinese), J. Glaciol. Geocryol., 253-257, 1991.

Mack, M. C., Bret-Harte, M. S., Hollingsworth, T. N., Jandt, R. R., Schuur, E. A., Shaver, G. R. and Verbyla, D. L.: Carbon loss from an unprecedented Arctic tundra wildfire, Nature, 475, 489-492,

https://doi.org/10.5194/essd-2024-187
Preprint. Discussion started: 3 June 2024

2011.

Mack, M. C., Walker, X. J., Johnstone, J. F., Alexander, H. D., Melvin, A. M., Jean, M. and Miller, S. N.: Carbon loss from boreal forest wildfires offset by increased dominance of deciduous trees, Science, 372, 280-283, doi: 10.1126/science.abf3903, 2021.

Michaelides, R. J., Schaefer, K., Zebker, H. A., Parsekian, A., Liu, L., Chen, J. Y., Natali, S., Ludwig, S. and Schaefer, S. R.: Inference of the impact of wildfire on permafrost and active layer thickness in a discontinuous permafrost region using the remotely sensed active layer thickness (ReSALT) algorithm, Environ. Res. Lett., 14, 035007, //doi: 10.1088/1748-9326/aaf932, 2019.

Miner, K. R., Turetsky, M. R., Malina, E., Bartsch, A., Tamminen, J., McGuire, A. D., Fix, A., Sweeney, C., Elder, C. D. and Miller, C. E.: Permafrost carbon emissions in a changing Arctic, Nat. Rev. Earth Environ., 3, 55-67, 2022.

Nelson, D. W., Sommers, L., Page, A. L., Miller, R. H. and Keeney, D. R., Total carbon, organic carbon, and organic matter Methods of Soil Analysis, Part 3, In: Sparks, D. L., Page, A. L., Helmke, P. A. and Loeppert, R. H. eds, Soil Science Society of America. Madison, WI, USA, pp. 539-552, 1982.

Nossov, D. R., Jorgenson, M. T., Kielland, K. and Kanevskiy, M. Z.: Edaphic and microclimatic controls over permafrost response to fire in interior Alaska, Environ. Res. Lett., 8, 035013, doi: 10.1088/1748-9326/8/3/035013, 2013.

Petrov, M. I., Fedorov, A. N., Konstantinov, P. Y. and Argunov, R. N.: Variability of permafrost and landscape conditions following forest fires in the Central Yakutian Taiga Zone, Land, 11, 496, doi: 10.3390/land11040496, 2022.

Ping, C. L., Michaelson, G. J., Kane, E. S., Packee, E. C., Stiles, C. A., Swanson, D. K. and Zaman, N. D.: Carbon stores and biogeochemical properties of soils under black spruce forest, Alaska, Soil Sci. Soc. Am. J., 74, 969-978, doi: 10.2136/sssaj2009.0152, 2010.

Șerban, R.D., Șerban, M., He, R., Jin, H., Li, Y., Li, X., Wang, X. and Li, G.: 46-Year (1973-2019) permafrost landscape changes in the Hola Basin, Northeast China using machine learning and object-based classification, Remote Sens., 13, 1910, doi: 10.3390/rs13101910, 2021.

Shur, Y. L. and Jorgenson, M. T.: Patterns of permafrost formation and degradation in relation to climate and ecosystems, Permafr. Periglac. Process., 18, 7-19, 2007.

Smith, S. L., O'Neill, H. B., Isaksen, K., Noetzli, J. and Romanovsky, V. E.: The changing thermal state of permafrost, Nat. Rev. Earth Environ., 3, 10-23, 2022.

Smith, S. L., Riseborough, D. W. and Bonnaventure, P. P.: Eighteen year record of forest fire effects on ground thermal regimes and permafrost in the Central Mackenzie Valley, NWT, Canada, Permafr. Periglac. Process., 26, 289-303, 2015.

Soil Survey Staff.: Keys to Soil Taxonomy, 12th Edition. Natural Resources Conservation Service, United States Department of Agriculture, Washington D.C., 2014.

Sun, L., Zhao, J. and Hu, H.: Effect of moderate fire disturbance on soil physical and chemical properties of *Betula platyphylla-Larix gmelinii* mixed forest, Sci. Silvae Sinicae, 47(2), 103-110, 2011. (in Chinese).

Turetsky, M. R., Abbott, B. W., Jones, M. C., Anthony, K. W., Olefeldt, D., Schuur, E. A. G., Koven, C., McGuire, A. D., Grosse, G., Kuhry, P., Hugelius, G., Lawrence, D. M., Gibson, C. and Sannel, A. B. K.: Permafrost collapse is accelerating carbon release, Nature, 569, 32-34, 2019.

Wang, H., Jin, H., Che, T., Li, X., Dai, L., Qi, Y., Huang, C., He, R., Zhang, J., Yang, R., Luo, D. and Jin, X.: Influences of snow cover on the thermal regimes of Xing'an permafrost in Northeast China in 1960s–2010s, Permafr. Periglac. Process., 35, 188-201, doi: 10.1002/ppp.2223, 2024.

https://doi.org/10.5194/essd-2024-187
Preprint. Discussion started: 3 June 2024

625 Westerling, A. L., Hidalgo, H. G., Cayan, D. R. and Swetnam, T. W.: Warming and earlier spring increase
626 Western U.S. forest wildfire activity, Science, 313, 940-943, doi: 10.1126/science.1128834, 2006.
627 Xu, W., Elberling, B. and Ambus, P. L.: Long-term summer warming reduces post-fire carbon dioxide
628 losses in an arctic heath tundra, Agric. For. Meteorol., 344, 109823, doi:
629 10.1016/j.agrformet.2023.109823, 2024
630 Yoshikawa, K., Bolton, W. R., Romanovsky, V. E., Fukuda, M. and Hinzman, L. D.: Impacts of wildfire
631 on the permafrost in the boreal forests of Interior Alaska, J. Geophys. Res., 108, 8148, doi:
632 10.1029/2001JD000438, 2003.
633 Zhao, L., Zou, D., Hu, G., Wu, T., Du, E., Liu, G., Xiao, Y., Li, R., Pang, Q., Qiao, Y., Wu, X., Sun, Z.,
634 Xing, Z., Sheng, Y., Zhao, Y., Shi, J., Xie, C., Wang, L., Wang, C. and Cheng, G.: A synthesis dataset
635 of permafrost thermal state for the Qinghai–Tibet (Xizang) Plateau, China, Earth Syst. Sci. Data,
636 13, 4207-4218, 2021.
637 Zhou, Y., Liang, L. and Gu, Z.: Effects of forest fire on hydro-thermal regime of frozen ground, the
638 northern part of the Da Hinggan Ling (in Chinese), J. Glaciol. Geocryol., 15, 17-26, 1993.